Modeling the Electromagnetic Radiation from Electrically Small Table-Top Products

TODD H. HUBING, MEMBER, IEEE, AND J. FRANK KAUFMAN, MEMBER, IEEE

Abstract—**Often, the most difficult radiated electromagnetic interference (EMI) problems with table-top products occur at frequencies where the maximum dimensions of the product are much smaller than a wavelength. Electrically small table-top products tend to be much more efficient radiation sources than dipole source models would predict and the radiation is generally much more difficult to contain than other types of EMI source models indicate. This paper investigates the ways in which electrically small sources radiate and proposes a technique for modeling electrically small table-top products that have power or signal cables. The *end-driven wire model*, as it is referred to in the paper, is a strategy for reducing the product to a form that is more readily analyzed. The result is a relatively simple configuration that includes only those parameters of the product that are of primary importance to the radiated EMI calculation.**

I. Background

SEVERAL YEARS ago an interesting observation was made concerning the radiated electromagnetic interference (EMI) from video display terminals. Measurements of several prototype terminals made by different manufacturers showed that the most significant EMI problems occurred between 30 and 100 MHz, the low end of the frequency range regulated by the FCC [1]. In every case, the EMI was due directly to the video signal, which was routed on a shielded cable from the logic board to the monitor. Since the fundamental video frequency of each display was below 30 MHz, it was not surprising that there was significant EMI at the lower harmonic frequencies where most of the signal energy was concentrated. However, each of the displays tested was very small relative to a wavelength at these frequencies and therefore a relatively inefficient radiator. It seemed reasonable to expect more radiation at the higher frequencies, since the decreasing energy in the video signal should have been compensated for by the increasing radiation efficiency of the source.

One explanation for the displays' ability to radiate at low frequencies was that currents on the relatively long attached cables were responsible for the radiation. Each display tested had a power cable and one coaxial signal cable attached that dropped to the ground plane below. However, attempts to isolate the cables from the display with ferrites and baluns had little effect on the radiated EMI. On the other hand, modifications made to the video circuit components including the signal driver, cable, and connectors tended to have a very significant impact on the radiation.

Manuscript received April 25, 1988; revised August 22, 1988.

T. H. Hubing is with IBM Communications Products Division, D75/061, Research Triangle Park, NC 27709. (919) 543-9896.

J. F. Kauffman is with North Carolina State University, Department of Electrical and Computer Engineering, Raleigh, NC 27650. (919) 737-2337.

IEEE Log Number 8825186.

Although the video circuit was apparently the primary EMI source in each of the display terminals tested, the radiation from each terminal was unique. Modifications to the video circuit that lowered the radiation from some displays increased the radiation from others. There was no clear correlation between the radiated EMI and any of the video circuit parameters that could be established based on the measured data. A radiation model for video display terminals was needed.

The video circuit in most displays is simple and electrically small. However, attempts to model the video circuit using a dipole modeling technique (see the Appendix) resulted in calculated values for the EMI that were much lower than measured values. In fact, even the most pessimistic of the video circuit dipole models tended to be well below the actual measurements.

The cables were thought to be contributing to the problem, but a better model was needed. Several radiation modeling procedures described in the literature [2]–[6] were researched and their applicability to the video display problem was examined. Unfortunately, none of these models correlated well with actual measurements of video displays. They were not detailed enough or did not focus on the correct radiation mechanism for video display products.

The goal of this work was to develop a relatively simple model that could be used to analyze and perhaps predict the radiation from video display terminals. Various radiation source configurations were analyzed on the computer using moment-method techniques and many of these were built and measured in the lab. The result of this work was a modeling technique that is referred to in this paper as *end-driven wire* modeling. This technique has proven to be very useful in the development and analysis of video display terminals and may be applied to other electrically small table-top products.

II. A Circuit Radiation Source

Two of the more popular moment-method programs for the analysis of time-harmonic electromagnetic radiation problems are the *Wires* program developed at Syracuse University [7]–[9] and *Numerical Electromagnetics Code* developed at Lawrence Livermore National Laboratory [10]. These FORTRAN programs accept wire configurations with voltage sources and loads as input and calculate parameters such as the radiation pattern, input impedance, and near electric field at designated points. The moment-method calculations presented in this paper were obtained using one or both of these programs.

Fig. 1 shows a simple circuit configuration consisting of

0018-9375/89/0200-0074$01.00

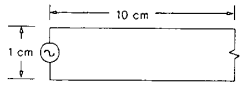

Frequency: 30 MHz
Source Voltage: 100 mV
Wire Radius: .5 mm

ELECTRIC FIELD STRENGTH AT A DISTANCE OF 3 METERS IN THE DIRECTION OF MAXIMUM RADIATION

	dB(uV/m)	
IN FREE SPACE	DIPOLE MODEL	MOMENT-METHOD MODEL
50-ohm circuit as shown:	18.0	19.2
50-ohm circuit (1mm wire radius):	18.0	19.8
50-ohm circuit (5 cm x 2 cm):	18.0	19.5
50-ohm circuit (load at top):	18.0	18.7
800-ohm circuit as shown:	0.4	4.2
800-ohm circuit (1mm wire radius):	0.4	5.8
800-ohm circuit (5 cm x 2 cm):	0.4	4.2
800-ohm circuit (load at top):	0.4	0.8
10000-ohm circuit as shown:	0.4	0.9
10000-ohm circuit (1mm wire radius):	0.4	3.2
10000-ohm circuit (5 cm x 2 cm):	0.4	0.8
10000-ohm circuit (load at top):	0.4	4.9
ABOVE A GROUND PLANE		
50-ohm circuit 80 cm above gnd plane:	24.0	24.0
800-ohm circuit 80 cm above gnd plane:	6.4	9.0
10000-ohm circuit 80 cm above gnd plane:	6.4	5.6

Fig. 1. Calculated field strengths for simple circuit configurations

a voltage source, load resistance, and two connecting wires. At 30 MHz, with a 100-mV source and a 50-Ω load, the maximum electric field strength (calculated using the *Wires* program), at a distance of 3 m is 19.2 dB (μV/m). This is in relatively good agreement with a simple dipole model calculation. The moment method model is about 1 dB higher primarily because of the near electric field, which the dipole model does not account for.

The moment-method model accounts for parameters such as the wire radius and the layout of the circuit. As Fig. 1 indicates, these parameters do not affect the maximum radiated field strength from the 50-Ω circuit very much, but they can have a significant effect on the radiation from high impedance circuits. This is because the open-circuit transmission line approximation (see (A10) in the Appendix) that is used in the derivation of the high-impedance dipole model is only valid for relatively symmetric circuits with wires that are thin relative to the wire spacing.

The 800-Ω circuit in Fig. 1 illustrates another problem with the dipole model. When the load resistance is neither very high nor very low, the radiation due to the uniform and nonuniform current distributions (see the Appendix) can add in phase in some directions causing the maximum field strength to be greater than predicted by the model.

EMI measurement procedures [11], [12] generally require that the equipment under test (EUT) be located above a ground plane. Using the dipole modeling technique, a common way of accounting for the ground plane is to add 6 dB to the calculation if the radiation is vertically polarized (the maximum electric field due to the source and its image in the ground plane). This is a relatively good approximation at low frequencies as the results in Fig. 1 indicate.

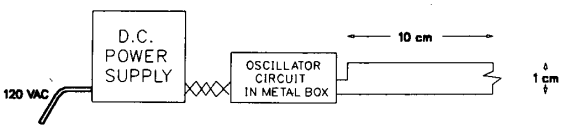

Fig. 2. Test setup for simple circuit radiation measurements.

Even though the dipole model is relatively crude, it predicts the radiation for each of the configurations in Fig. 1 within 6 dB. This is relatively good accuracy for an EMI prediction. If sources of EMI such as computers and computer peripherals could be approximated by a collection of simple, noninteracting circuits similar to the one in Fig. 1, the error associated with the dipole model would probably be acceptable.

However, circuits are rarely isolated from nearby objects that affect the radiated fields. Consider the test setup diagrammed in Fig. 2. A dc power supply is used to power a circuit containing an oscillator and a CMOS NAND gate. The circuit is packaged in a metal box. The output from the NAND gate is a trapezoidal wave with harmonics at multiples of 2.0 MHz. The amplitudes and frequencies of these harmonics are very stable making this a good reference source [13]. The NAND gate output drives a 10 cm × 1 cm, 50-Ω circuit similar to the one in Fig. 1. The oscillator frequency is 2.0 MHz and the output of the NAND gate has frequency components at harmonics of 2.0 MHz as expected. The amplitude of the harmonic at 30 MHz is measured with a spectrum analyzer and is found to be 100 mV.

Although this is a very poor circuit design from an EMI standpoint, the calculated field strength for this circuit, using the dipole model and adding 6 dB for the effect of the ground plane, is only 24 dB (μV/m). A careful measurement of this configuration shows that the actual maximum electric field strength at 30 MHz is 59 dB (μV/m).

Why is the measured field so much higher than the dipole model prediction? Refer to the model in Fig. 3. It is similar to the circuit in Fig. 1, but a wire has been added between the circuit's *ground* and the ground plane. With the wire dropping to within 1 cm of the ground plane, the field strength (calculated using the Numerical Electromagnetics Code) from the 50-Ω circuit is 36.2 dB (μV/m), 12 dB higher than from the circuit alone. When the wire is attached to the ground plane, the field strength increases another 6.4 dB. A 2.8-m attached wire (0.8 m of cable oriented vertically and 2 m of cable oriented horizontally) increases the calculated field strength to 57.4 dB (μV/m).

Clearly, an attached wire can have a significant effect on the radiated fields. The test setup illustrated in Fig. 2 includes a power cord that is (indirectly) connected to the radiation source. Dipole models do not account for the presence of the wire. A moment-method analysis approach can be used, but first it is necessary to understand what parameters of the configuration to be analyzed have a significant impact on the radiation. This is necessary so that essential features of the configuration are not ignored when the equipment to be modeled

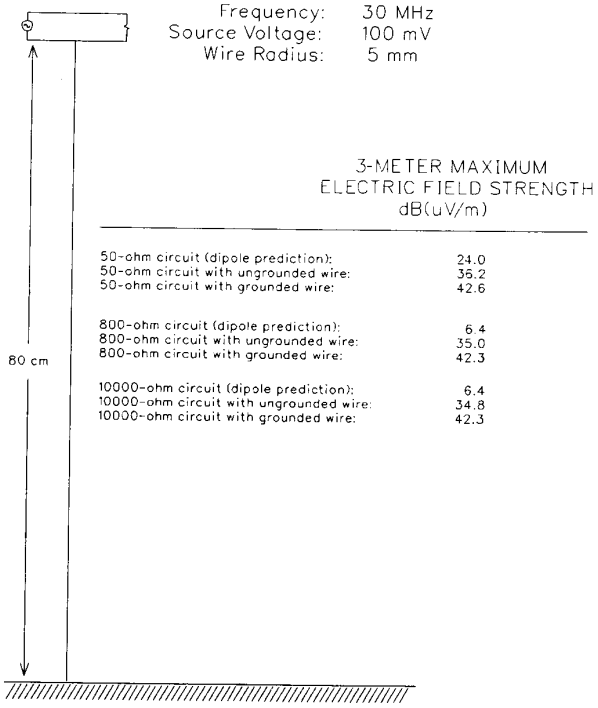

Fig. 3. Simple circuit with attached wire.

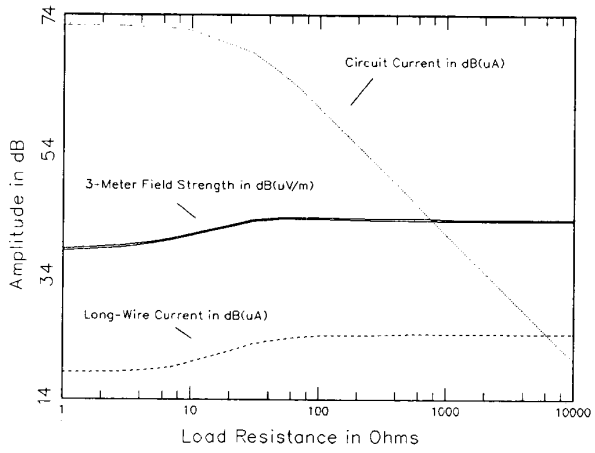

Fig. 4. Field strength and currents as a function of load resistance.

is reduced to a form suitable for input to a moment-method program.

III. Small Sources Attached to Long Wires

Fig. 3 suggests that the radiation from a circuit with a relatively long attached wire is somewhat independent of the load impedance. This becomes even more apparent when the maximum radiated field strength from the configuration in Fig. 3 is plotted as a function of load resistance as in Fig. 4. The circuit current and the current at the base of the long wire are also plotted as a function of load resistance. Note that the radiated field strength closely tracks the long wire current and is relatively independent of the circuit current. This suggests that the overall current distribution can be broken into two components. One component (see Fig. 5) is uniformly distributed around the loop portion of the circuit. The other component is zero at the load and increases linearly to a finite value at the source. This component of the current continues down the long wire and its distribution on the wire depends on the length of the wire and how the wire is terminated.[1] Fig. 6 lists the currents calculated for the configuration in Fig. 3 and shows how the overall current distribution can be factored into these two components.

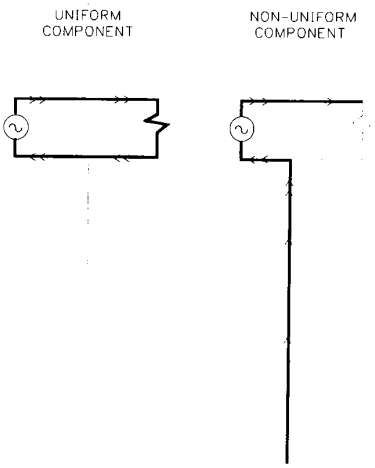

Fig. 5. Components of current in a circuit with an attached wire.

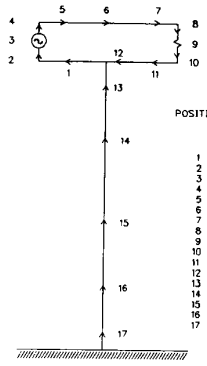

POSITION	TOTAL CURRENT (uA) REAL	TOTAL CURRENT (uA) IMAG	UNIFORM COMPONENT (uA) REAL	UNIFORM COMPONENT (uA) IMAG	NON-UNIFORM COMPONENT (uA) REAL	NON-UNIFORM COMPONENT (uA) IMAG
1	1635.7	-760.4	1629.8	-784.1	6.0	23.7
2	1635.5	-758.7	1629.8	-784.1	5.8	25.5
3	1635.5	-757.8	1629.8	-784.1	5.7	26.4
4	1635.4	-759.2	1629.8	-784.1	5.7	24.9
5	1635.0	-763.8	1629.8	-784.1	5.3	20.4
6	1633.7	-771.5	1629.8	-784.1	4.0	12.7
7	1631.7	-778.8	1629.8	-784.1	2.0	5.3
8	1630.3	-782.9	1629.8	-784.1	0.5	1.3
9	1629.8	-784.1	1629.8	-784.1	0.0	0.0
10	1630.3	-783.5	1629.8	-784.1	0.5	0.7
11	1631.0	-782.2	1629.8	-784.1	1.2	2.0
12	1632.0	-779.3	1629.8	-784.1	2.3	4.9
13	3.4	15.7	0.0	0.0	3.4	15.7
14	3.4	15.5	0.0	0.0	3.4	15.5
15	3.1	14.2	0.0	0.0	3.1	14.2
16	3.3	14.5	0.0	0.0	3.3	14.5
17	3.3	14.6	0.0	0.0	3.3	14.6

Fig. 6. Current component distributions for a long-wire configuration.

In most practical configurations, the contribution of the uniform component of the current to the radiated field is relatively insignificant. The radiation can be modeled with sufficient accuracy by accounting only for those parameters that affect the nonuniform (i.e., long wire) component of the current. For example, the circuit in Fig. 7(a) can be reduced to the configurations in Fig. 7(b) or Fig. 7(c) without significantly changing the calculated field strength. The load resistance and the circuit's shape are completely neglected, and yet this simple

[1] A third component can be defined that is zero at the load, has a maximum at the source, and goes to zero again at the other side of the load. This component with the other two comprise a complete set but the third component will generally be insignificant relative to the long-wire component for electrically small circuits.

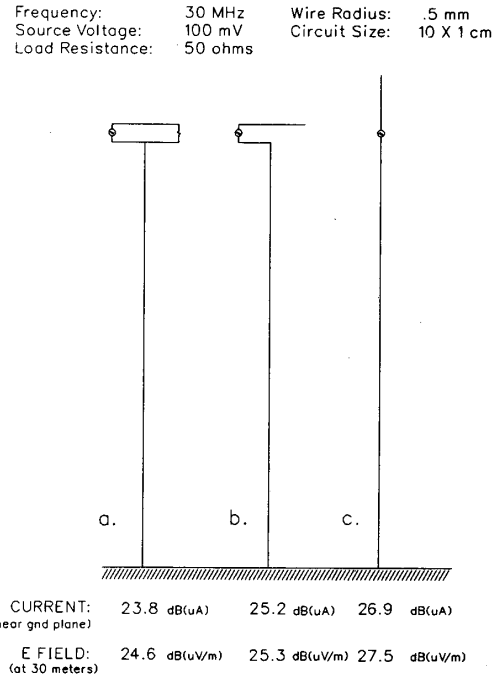

Fig. 7. Reducing a circuit to its end-driven wire radiation equivalent.

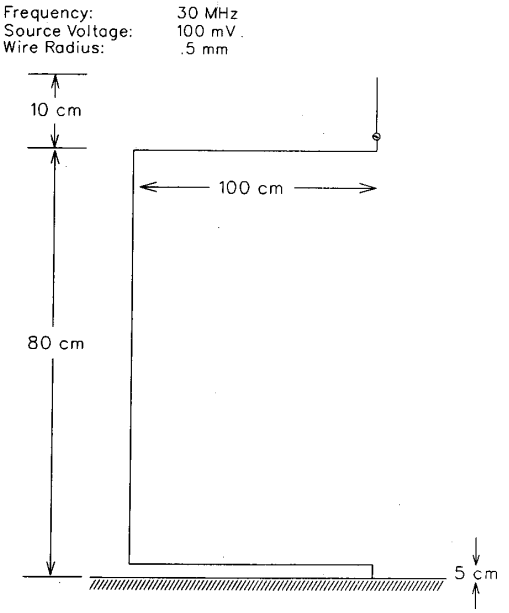

Fig. 8. End-driven wire model of test circuit with dc power supply.

model consisting of a wire driven near one end estimates the radiated electric field strength within 3 dB.

This raises some important questions. Can *real* sources of EMI that are small relative to a wavelength and attached to long wires be reduced to an end-driven wire model like the one in Fig. 7(c) for predicting the radiated fields? If so, what parameters of the configuration have to be taken into account and when is this type of model valid?

Refer back to the test setup in Fig. 2. This is somewhat representative of a realistic EMI source in that it contains an oscillator, digital circuits, and a power supply. The model suggests that the radiation is primarily due to common-mode[2] currents induced on the power cord. To confirm this, the power supply was removed from the configuration. A built-in battery pack continued to supply power to the circuit and the voltage at the output of the NAND gate was still 100 mV. The 3-m electric field strength calculated for this configuration, using either the dipole model or a moment method technique, was about 24 dB (μV/m). The measured field strength was 25 dB (μV/m), indicating that (in the absence of a power cord) there is good agreement between the models and the measurement.

The total length of the power cord, including the length of the power supply and the dc voltage supply wires, was approximately 280 cm. The line cord ran horizontally across the table for 1 m then dropped to the ground plane and was plugged in to a line impedance stabilization network [11] located directly under the source circuit. Using the crude model illustrated in Fig. 8, the calculated field strength at 3 m is 61.9 dB (μV/m). This is within 3 dB of the actual measurement.

But what about small EMI sources that do not have cables or whose radiation is not dominated by the common-mode currents induced on the cables? An end-driven wire model could certainly not be applied to a device without cables, but cable-less computing devices are the exception. The FCC EMI measurement procedure [11] requires that any device with a place to plug a cable must be tested with a cable. Even a battery-powered calculator has to be tested with a power cord if a port has been provided for charging the batteries. Therefore, restricting the model to EMI sources with attached cables is not a severe limitation.

Situations where the radiation from an electrically small source is not dominated by the common-mode currents induced on the cables are also rare. Electrically small circuits that are capable of exceeding the FCC requirements on their own tend to radiate much more with a cable. For example, a battery-powered reference source with a 23-cm antenna radiates at or near the FCC Class A limit between 30 and 100 MHz as shown in Fig. 9. However, with a 1-m wire attached, the amplitude of the radiated field changes dramatically. The radiated levels at every frequency are affected.

If there were some way to isolate the cable from the source and thereby reduce the cable currents without affecting the circuit currents, situations where the common-mode currents did not dominate would be common and the end-driven wire model would not be useful. Isolation techniques such as this exist in theory, but are only moderately successful in practice. As a result, common-mode currents on cables tend to dominate the radiation from most electrically small table-top products. The problem of effectively isolating a radiation source

[2] Common-mode current is the component of the cable current that flows in the same direction on all conductors as opposed to differential or normal-mode current which flows in opposite directions using different conductors in the same cable.

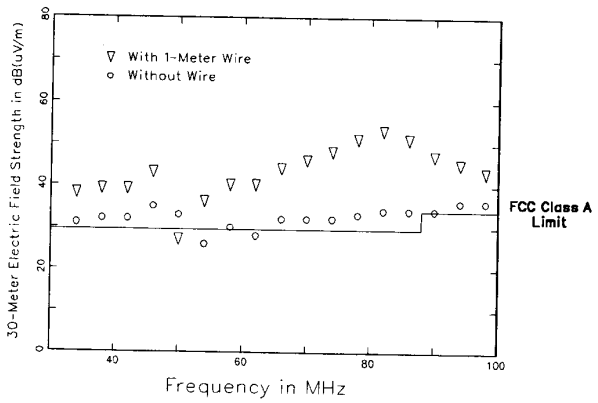

Fig. 9. Measured EMI from a circuit attached to a 23-cm antenna.

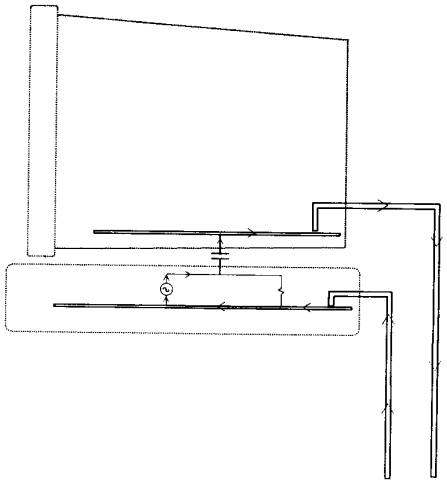

Fig. 10. Example of how one cable may be driven relative to another.

from power and signal cables will be discussed in the next section.

There is one class of electrically small table-top products that cannot be modeled with an end-driven wire technique. Products with more than one attached cable where one cable is being *driven* relative to another (see Fig. 10) are relatively complex radiation sources. Products that drive the cables in this manner can have severe EMI problems and generally it is desirable to tie all of the cable shields together with a low-impedance connection in order to avoid this problem. When the cable shields are connected, the end-driven wire model can be applied to products with more than one cable by replacing the bottom section of the model with multiple wires connected just below the source.

IV. Filters, Ferrites, and Baluns

Referring back to the test setup in Fig. 2, a low-pass filter (0.01-μF capacitor and ferrite beads) was placed on the two wires carrying the dc power between the power supply and the circuit. The radiated electric field at 30 MHz was unaffected. The reason for this is simply that filters of this type do nothing to reduce common-mode currents induced on the cables. The

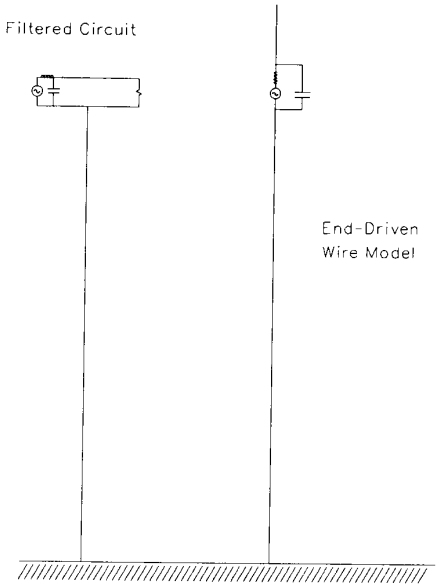

Fig. 11. End-driven wire model of a filtered circuit.

nonuniform component of current (Fig. 5) is unaltered by the presence of the filter. If a similar filter had been placed in the circuit itself as shown in Fig. 11, a reduction in the radiated field would be expected. Note that the filter is only effective to the extent that it reduces the high-frequency components of the signal.

A large ferrite core was placed on the power cord of the configuration in Fig. 2 and the radiated electric field strength was measured again. The amplitude of the field was 59 dB (μV/m), approximately the same as it had been before adding the ferrite. In order to understand the reason for this, it helps to refer to the end-driven wire model. A moment-method analysis of the configuration in Fig. 8 reveals that the impedance (ratio of open-circuit voltage to short-circuit current) in the vicinity of the source is very high. This is not surprising since, near the wire's termination, a relatively high voltage would be required to get even a small amount of current flow. At the point in this model where the ferrite was added (about 10 cm below the source), the calculated impedance is around $j3000$ Ω. Ferrite devices are not very effective in high impedance situations since the reduction in common-mode current is proportional to the change in the overall impedance caused by the addition of the ferrite. In this particular case, the measured impedance of the ferrite turned out to be only $38 + j53$ Ω at 30 MHz. The calculated change in the common-mode current is approximately

$$20 \log \left| \frac{j3000}{38 + j52 + j3000} \right| = -.15 \text{ dB}. \quad (1)$$

As Fig. 12 indicates, the impedance at points near one end of a wire above ground tends to be very high at most frequencies. The frequency f_1 in Fig. 12 is the frequency at which the total wire length (including the image) corresponds to a half-wavelength. f_2 is the frequency at which the length of wire between the measurement point and its image is a

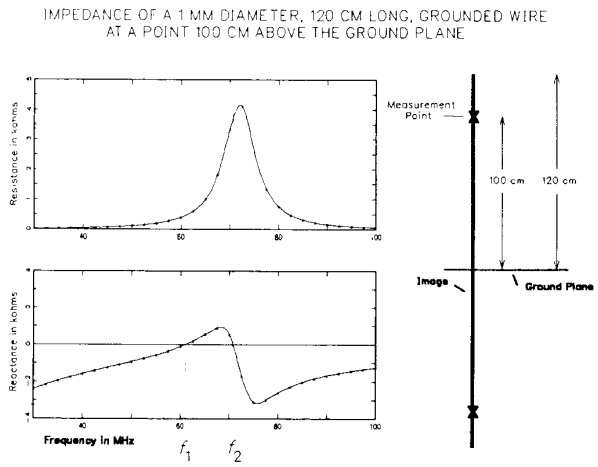

Fig. 12. Resistance and reactance near one end of a long wire.

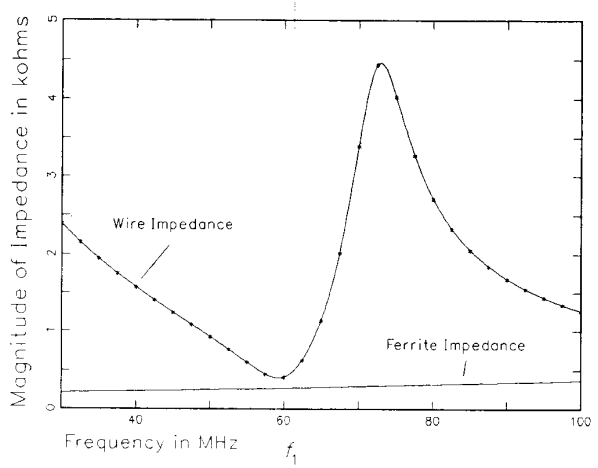

Fig. 13. Magnitude of the impedance near one end of a long wire.

half-wavelength. At points near the end of the wire, these frequencies are close to each other and the range of frequencies with a low reactance is narrow. At the frequency f_2, the real part of the impedance is very high. Therefore, the only frequencies at which a ferrite can be expected to attenuate common-mode currents are in the narrow band around f_1, where the magnitude of the wire impedance is comparable to that of the ferrite's impedance (see Fig. 13). Fig. 14 shows a plot of the radiated electric field from the wire in Fig. 12 both with and without a ferrite[3] located at the *measurement point*. The ferrite reduced the radiated electric field strength near resonance by about 3 dB. At other frequencies it was relatively ineffective.

Ferrites are often found on electrically small products because radiation at resonant frequencies is often a problem. Since they can affect the common-mode currents near resonance, ferrites should be included in the end-driven wire model when they are present in the product. However, despite

[3] The ferrite was modeled with a 192-Ω resistor and a 500-nH inductor in series.

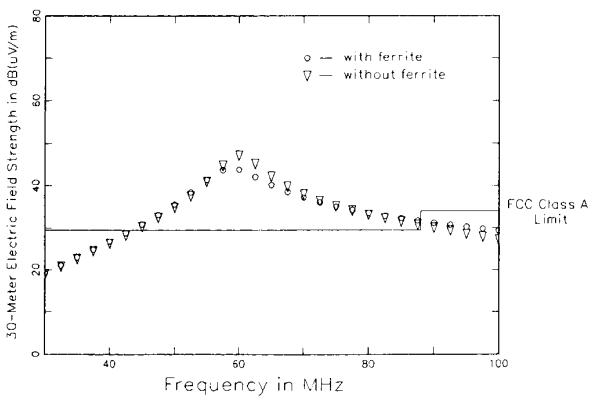

Fig. 14. Ferrite's effect on the radiation from the 120-cm wire.

the presence of the ferrite, the radiation at each frequency in Fig. 14 is dominated by the current on the wire below the point where the ferrite is located. Ferrites do not isolate electrically small sources from cables well enough to prevent the *nonuniform* component of current from dominating.

Baluns and isolation transformers are also relatively ineffective means of isolating electrically small sources from their cables. As in the case of the ferrites, the reason is due to the high impedance in the vicinity of the source. Even very good isolation transformers have a certain amount of leakage capacitance. A transformer with just 10 pF of capacitance, for example, would put an additional reactance of only about 530 Ω on a wire at 30 MHz. If this transformer were placed at the *measurement point* in Fig. 12, the expected reduction in the common-mode current would be only

$$\text{net decrease} = \left| \frac{\text{wire impedance}}{\text{wire impedance} + \text{transformer impedance}} \right|$$

$$= \left| \frac{20 - j2391}{20 - j2391 - \dfrac{j}{2\pi(3 \times 10^7)(10 \times 10^{-12})}} \right|$$

$$= 0.82$$

$$= -1.7 \text{ dB}. \tag{2a}$$

At 60 MHz (near resonance), where the wire impedance is close to its lowest value, the additional isolation provided by the transformer is still minimal

$$\text{net decrease} = \left| \frac{396 - j113}{396 - j113 - \dfrac{j}{2\pi(6 \times 10^7)(10 \times 10^{-12})}} \right|$$

$$= 0.75$$

$$= -2.5 \text{ dB}. \tag{2b}$$

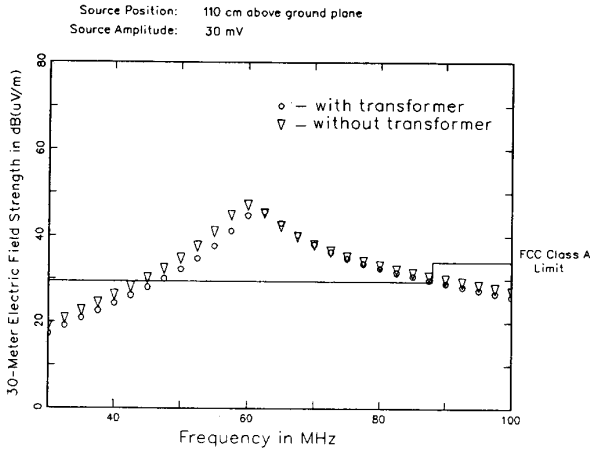

Fig. 15. Isolation transformer's effect on the radiation from the 120-cm wire.

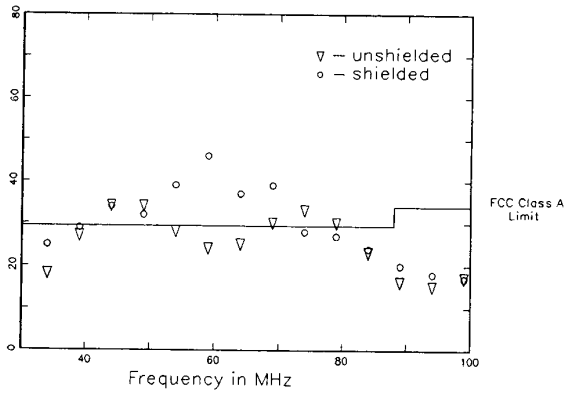

Fig. 16. Radiation from a small circuit with and without a shield.

These small reductions in the common-mode currents are reflected in the calculation of the radiated electric field strength. Fig. 15 shows the calculated field strength for the wire in Fig. 12 with and without a 10-pF capacitance located at the *measurement* point.

V. Shields

Another way to try to isolate a circuit from power and signal cables is to shield the circuit. In theory, a circuit completely surrounded by a conductive enclosure is unable to induce current on an attached cable. However, completely sealed metal enclosures are not very practical. Generally, shielded enclosures have holes for displays, connectors, ventilation, etc. Many devices are shielded on only two or three sides and often a shield consists of a single metal plate.

How effective are partial shields for reducing the common-mode currents induced on wires attached to electrically small circuits? Fig. 16 shows the measured EMI from the previously mentioned CMOS NAND gate circuit with and without a shield. For this measurement, the entire circuit was laid out on a breadboard over a 29 × 23 cm aluminum plate. The breadboard circuit was placed on a table 80 cm above a ground plane. The circuit's *ground* was connected to the aluminum

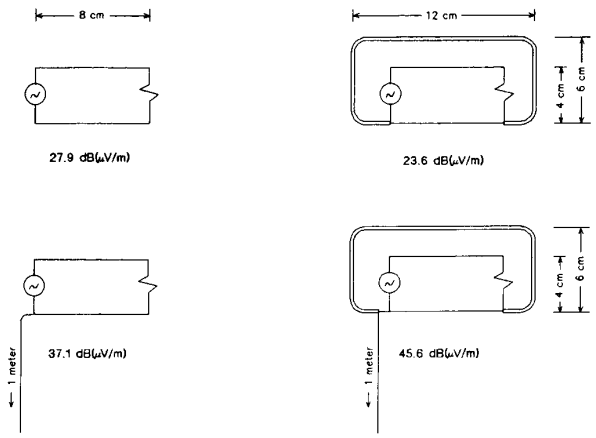

Fig. 17. Wire model of circuit with and without a shield.

plate and a 1-m wire was dropped from the plate to the ground plane. The circuit output was terminated with a 1000-Ω resistor. The shield consisted of three thin pieces of brass. Each piece had four to six legs that plugged into the breadboard connecting to circuit ground. The three shields completely covered the circuitry on the breadboard.

As Fig. 16 indicates, the radiation from the shielded circuit was significantly higher than that from the unshielded circuit. In order to help understand how this can happen, we again go back to the moment-method analysis of the end-driven wire model.

Four circuit configurations are illustrated in Fig. 17. The first configuration is a simple 50-Ω circuit. The radiated 30-m field strength from this circuit is 27.9 dB (μV/m). The second configuration is the same circuit with a 4-mm diameter wire attached. The thick grounded wire essentially encloses the circuit in the plane of the measurement in a manner similar to the shield in the example of Fig. 16. As expected, the radiated field strength is lower (by 4.3 dB). The third configuration is similar to the first with a 1-m wire attached. Its 30-m field strength is 37.1 dB (μV/m). The addition of the same thick wire to this configuration, however, actually increases the radiated field strength by 8.3 dB.

Breaking the total current into uniform and nonuniform components, it was found that the nonuniform component extends beyond the load resistance and up onto the shield wire as illustrated in Fig. 18. This results in a lower input impedance at the source and increases the amplitude of the nonuniform component of the current. A shield or anything metallic in the vicinity of the circuit termination can have this effect.

Clearly one objective in the design of a shield is to avoid *driving* the shield and thereby enhancing the ability of the source to put the common-mode current on the cables. This suggests the possibility of using a flat plate attached to the circuit ground between the circuit and the attached wire as shown in Fig. 19. This configuration is found in many practical situations and it is roughly equivalent to a circuit on a printed circuit board with internal voltage and ground planes.

If the plate in Fig. 19 were infinite, the amplitude of the current on the attached wire would be zero. In practice, how-

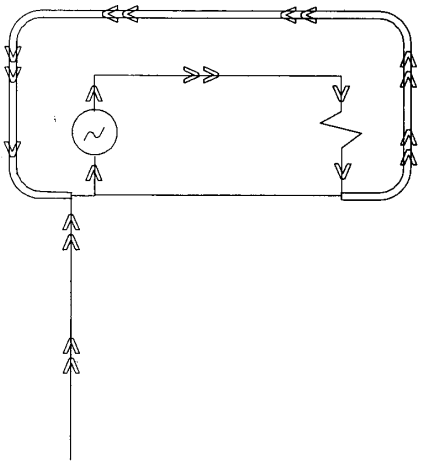

Fig. 18. Nonuniform component of current on wire shield example.

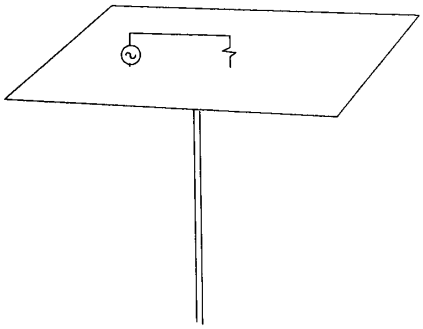

Fig. 19. Model of circuit with attached wire mounted above a ground plate.

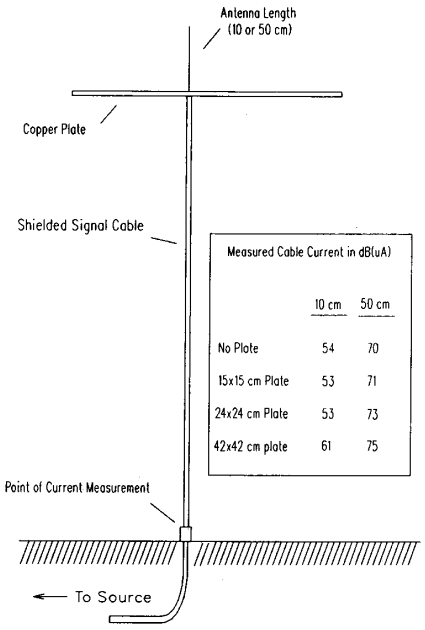

Fig. 20. Physical model of an end-drive wire with ground plate.

ever, these ground plates have dimensions much smaller than a wavelength. It is not obvious how a plate that is large relative to the dimensions of the circuit, but small relative to a wavelength, will affect the common-mode currents on an attached cable.

Moment-method modeling of this configuration presents a complex problem that is investigated in [14]. A quick measurement, however, provides us with an indication of how effective this shielding technique is. The shield of a 1-m-long coaxial cable is attached to a copper plate (1 m off the floor) at one end and a metal floor tile at the other end (see Fig. 20). A short monopole antenna is mounted above the copper plate and connected to the center conductor of the coaxial cable. A 30-MHz signal source is connected to the other end of the coax. The result is a configuration equivalent to an end-driven wire model of the circuit in Fig. 19. As the table in Fig. 20 indicates, the shield does not reduce the common-mode currents on the long wire. In fact, the larger shields resulted in higher levels of common-mode current. The reason for this increase [14] is that common-mode currents were forced to go around the shield, which lowered the resonant frequency of the configuration and reduced the input impedance at the source.

In general, a shield of this type is not an effective way of isolating a source from its power and signal cables. Common-mode cable currents are generally the dominant source of the radiated electric fields from electrically small table-top sources despite the presence of ferrites, filters, baluns, transformers, or shields designed to keep these currents off the attached cables.

VI. The Modeling Procedure

The analysis of electrically small table-top products is a two-step process:

1) Reduce the product to its end-driven wire equivalent, complete with lumped-element components and shields.
2) Analyze the end-driven wire model using a moment-method technique.

Reducing a product to its end-driven wire equivalent is relatively straightforward once the source circuit has been identified. Circuit analysis programs, scope probes, or close-field probes may be used to locate this circuit. If there is more than one source, separate end-driven wire models should be derived and the sources should be analyzed individually.

Once the source is identified, all components that do not have an effect on the common-mode current can be neglected. Parameters that generally have the biggest effect on the common-mode current are the signal source (e.g., a TTL gate), the cables, metal plates, and any lumped-element components such as ferrites that are in series with the common-mode current path. Details of the circuit's termination can usually be neglected except for the effect that the termination has on the source's signal amplitude.

Once the product is in the form of an end-driven wire model, it can be analyzed using a moment-method analy-

sis technique [7]–[10], [14]. Metal plates and shielded cables present unique problems beyond the scope of this paper, but they do not prevent the end-driven wire model from being analyzed using moment-method techniques [14], [15].

The model does not eliminate the necessity of measuring the product. However, it has proven to be very useful for estimating how good one particular design is relative to another or what impact a change in the design will have on the EMI. The accuracy of the model is limited primarily by three factors:

1) The ability of the user to identify the correct source circuit.
2) The accuracy of the source amplitude used in the model. (It is generally best to measure the source component on a spectrum analyzer, although the measured spectrum may change when the source is operating under different conditions.)
3) The fact that the exact resonant frequencies of the end-driven wire may be different from the resonant frequency of the product. (The exact resonant frequency is often dependent on parameters that the end-driven wire model ignores.)

Radiation models alone can be used to recognize the potential for an EMI problem early in the design stage, but they are most useful when they are compared with actual measurements. Understanding the reasons that the model results disagree with the measurements is the key to understanding how the product radiates. In situations where a product behaves very differently than predicted by the end-driven wire model, it is generally because the wrong source is assumed or because the source is indirectly driving another cable as shown in Fig. 10. The model helps the design engineer to recognize and correct these situations.

VII. Conclusions

Electrically small circuits are very inefficient sources of radiation. When these circuits are operating in the vicinity of relatively long power or signal cables, the currents induced on the cables are generally the primary sources of electromagnetic radiation. This is true even when the circuit has been *isolated* from the cables with ferrites, filters, transformers, or metal plates.

The *end-driven wire* modeling technique takes advantage of this fact by discarding all of the configuration parameters that do not significantly affect the common-mode currents induced on the power and signal cables. This results in a relatively simple configuration that can be analyzed with general-purpose moment-method techniques. End-driven wire models are relatively accurate because they focus on the primary radiation mechanism in electrically small table-top products and the cables are modeled as antennas instead of using circuit or transmission-line representations. This modeling technique is particularly useful for analyzing early designs or evaluating potential EMI "fixes."

The results that have been presented illustrate the importance of the circuit's environment in determining the overall radiation. A knowledge of how electrically small sources interact with relatively large objects near them is critical to the analysis of many radiation problems. The end-driven wire model cannot be used to analyze products that are not electrically small at the frequency of interest, products without cables, floor-standing products, or well-shielded products. However, the principles used in the derivation and understanding of this model are basic and can be applied in many situations.

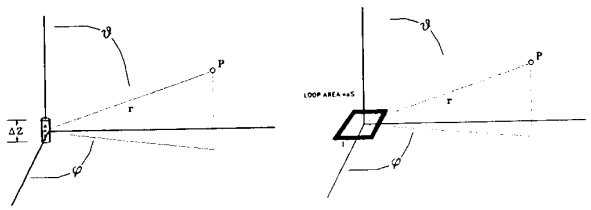

Fig. 21. Ideal dipole radiation sources.

Appendix

Dipole Radiation Modeling

Radiation sources with dimensions much smaller than a wavelength are often modeled as ideal dipole sources. An ideal electric dipole can be represented by a short uniform current element as shown in Fig. 21(a). The fields emanating from an electric dipole are described by the following equations [16]:

$$E_\theta = \frac{I(\Delta z)\eta\beta^2}{4\pi} e^{-j\beta r}\left[\frac{j}{\beta r} + \frac{1}{(\beta r)^2} - \frac{j}{(\beta r)^3}\right] \sin\theta \quad \text{(A1)}$$

$$E_r = \frac{I(\Delta z)\eta\beta^2}{4\pi} e^{-j\beta r}\left[\frac{2}{(\beta r)^2} - \frac{2j}{(\beta r)^3}\right] \cos\theta \quad \text{(A2)}$$

$$H_\phi = \frac{I(\Delta z)\beta^2}{4\pi} e^{-j\beta r}\left[\frac{j}{(\beta r)} + \frac{1}{(\beta r)^2}\right] \sin\theta \quad \text{(A3)}$$

where β is the wavenumber and η is the intrinsic impedance in free-space. An ideal magnetic dipole can be represented by a very small electric current loop as shown in Fig. 21(b). The fields associated with a magnetic dipole are

$$E_\phi = -\frac{I(\Delta S)\eta\beta^3}{4\pi} e^{-j\beta r}\left[\frac{-1}{\beta r} + \frac{j}{(\beta r)^2}\right] \sin\theta \quad \text{(A4)}$$

$$H_r = \frac{I(\Delta S)\beta^3}{4\pi} e^{-j\beta r}\left[\frac{2j}{(\beta r)^2} + \frac{2}{(\beta r)^3}\right] \cos\theta \quad \text{(A5)}$$

$$H_\theta = \frac{I(\Delta S)\beta^3}{4\pi} e^{-j\beta r}\left[\frac{-1}{(\beta r)} + \frac{j}{(\beta r)^2} + \frac{1}{(\beta r)^3}\right] \sin\theta \quad \text{(A6)}$$

Note that the field components have terms that are proportional to $1/r$ (far-field) and terms that are proportional to $1/r^2$ and $1/r^3$ (near-field). Although the near-field terms must be considered in order to predict how a source will interact with nearby objects (e.g., other sources or shields), dipole modeling techniques generally assume that the source is unaffected by its surroundings and therefore only the far-field terms are considered. In the far-field, the maximum electric

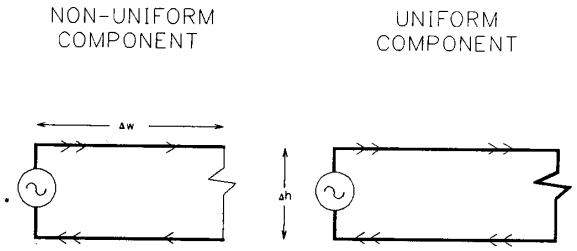

Fig. 22. Components of current distribution in a small circuit.

field strength from a magnetic dipole is given by

$$|E_\phi|_{\max} = \frac{I(\Delta S)\eta\beta^2}{4\pi r}. \tag{A7}$$

The maximum electric field strength from an electric dipole is given by

$$|E_\theta|_{\max} = \frac{I(\Delta z)\eta\beta}{4\pi r}. \tag{A8}$$

The current distribution in a simple electrically small circuit can be broken down into two components as illustrated in Fig. 22. One component is uniform throughout the circuit and the other component has a maximum value at the source and is zero at the load. The total current distribution is a sum of these two components.

The uniform current component can be modeled as a magnetic dipole and the maximum radiated electric field strength can be calculated by substituting V/R for I in (A7). The nonuniform current component is modeled as an open-circuit transmission line. The radiation is dominated by the section of the circuit containing the source, which is a single wire element with length Δh. Modeling this segment as an electric dipole source, the maximum electric field strength can be calculated using (A8). The dipole current is approximately the source current

$$I_s \frac{V}{|Z_{in}|} \tag{A9}$$

where Z_{in} is the input impedance of a short transmission line with length Δw

$$|Z_{in}| = \frac{\eta}{\beta\Delta w}. \tag{A10}$$

Combining (A8)–(A10) and noting that $\Delta h \times \Delta w = \Delta S$, the following expression for the maximum electric field strength due to the nonuniform current component is obtained:

$$|E_\theta|_{\max} = \frac{V(\Delta s)\beta^2}{4\pi r}. \tag{A11}$$

Therefore, the overall maximum radiated field strength from an arbitrary small circuit with both current components present is

$$|E|_{\max} = \begin{cases} \dfrac{V\Delta S\eta\beta^2}{4\pi r R}, & R < \eta \\ \dfrac{V\Delta S\beta^2}{4\pi r}, & R > \eta. \end{cases} \tag{A12}$$

Note that in low-impedance circuits, the uniform current component dominates and the radiation is similar to that of a magnetic dipole. In high-impedance circuits, the nonuniform component dominates and the radiation is similar to that from an electric dipole. The maximum electric field strength is independent of the load impedance when the load impedance is greater than the intrinsic impedance of free-space.

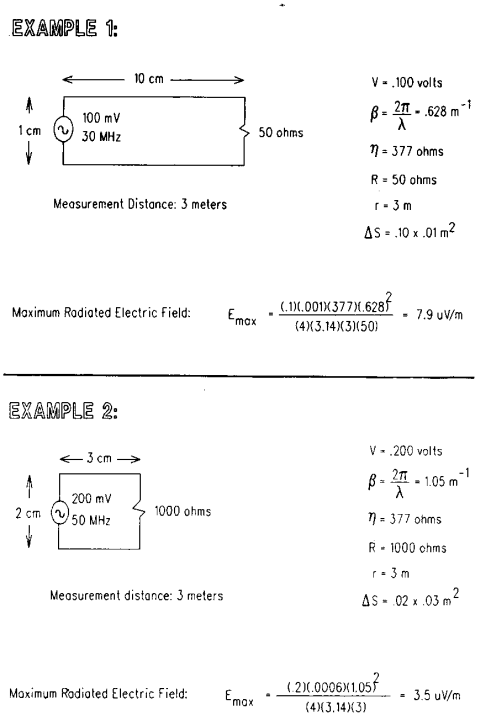

Fig. 23. Two dipole modeling examples.

Fig. 23 outlines the procedure for calculating the maximum radiated field strength from two sample circuits. The dipole modeling technique is simple to use and helps the user to understand what parameters of a circuit could be changed in order to reduce the radiated field strength. Even though this technique neglects the effects of parameters such as wire radius, circuit shape, and the relative placement of circuit components, it provides a fairly accurate estimate of the maximum radiated field from simple circuit configurations.

The primary limitation of the dipole modeling technique stems from the fact that the near-field terms in (A1)–(A6) are not utilized. Most practical circuits are located in the presence of other circuits, wires, and metallic surfaces. These nearby objects can have a very significant effect on the radiation. The interaction between the source circuit and other objects is generally too complex to be adequately accounted for in the dipole model.

References

[1] *U.S. Code of Federal Regulations,* title 47, part 15, subpart J.
[2] *C.I.S.P.R. Specification for Radio Interference Measuring Apparatus and Measurement Methods,* C.I.S.P.R. Pub. 16, 1977, appendix F.
[3] M. Costa et al., "On radiation from printed circuits," *IEEE Int. Symp. EMC,* # 81CH1675-8, pp. 246–249, 1981.

[4] D. R. J. White, *EMI Control in the Design of Printed Circuit Boards and Backplanes.* Gainesville, VA: Don White Consultants, 1982, sec. 4.3.
[5] ——, *EMI Control Methodology and Procedures.* Gainesville, VA: Don White Consultants, 1982, ch. 10.
[6] R. Raut, "On the computation of electromagnetic field components from a practical printed circuit board," *IEEE Int. Symp. Electromagn. Compat.*, # 86CH2294-7, pp. 161–165, 1986.
[7] H. H. Chao and B. J. Strait, "Computer programs for radiation and scattering by arbitrary configurations of bent wires," AFCRL-70-0374, Sci. Rep. 7, Sept. 15, 1970.
[8] D. C. Kuo and B. J. Strait, "Improved programs for analysis of radiation and scattering by configurations of arbitrarily bent thin wires," AFCRL-72-0051, Sci. Rep. 15, Jan. 15, 1972.
[9] M. D. Tew, "Correction to WIRES program," *IEEE Trans. Antennas Propagat.*, vol. AP-33, pp. 450–451, May 1975.
[10] G. J. Burke and A. J. Poggio, *Numerical Electromagnetics Code (NEC)—Method of Moments,* Naval Ocean Syst. Center, San Diego, CA, NOSC Tech. Document 116, Jan. 1981.
[11] *FCC Procedure for Measuring RF Emissions from Computing Devices,* FCC/OET MP-4 (1987), July 1987.
[12] *Limits and Methods of Measurement of Radio Interference Characteristics of Information Technology Equipment,* C.I.S.P.R. Pub. 22, 1985.
[13] T. H. Hubing, "A stable and predictable source of electromagnetic radiation," IBM Tech. Rep. # 29.0671, Jan. 1987.
[14] ——, "Modeling the electromagnetic radiation from electrically small sources with attached wires," Ph.D. dissertation, North Carolina State Univ., chs. 3 and 4, May 1988.
[15] H. Hejase *et al.*, "Shielding effectiveness of 'pigtail' connections," *IEEE Int. Symp. Electromagn. Compat.*, # 87CH2487-7, pp. 253–259, 1987.
[16] B. E. Keiser, *Principles of Electromagnetic Compatibility.* Dedham, MA: Artech House, 1989, p. 28.